ISSN 1070-3632, Russian Journal of Bioorganic Chemistry, 2023, Vol. 49, No. 6, pp. 1216–1228. © Pleiades Publishing, Ltd., 2023.
Russian Text © The Author(s), 2023, published in Bioorganicheskaya Khimiya, 2023, Vol. 49, No. 6, pp. 575–590.

Radiopharmaceuticals for Non-Glucose-Specific Oncology (PET and SPECT) (A Review)

E. D. Belitskaya[a,b,*], V. A. Dimitreva[a,b], A. N. Kozlov[a], V. A. Oleinikov[a,b], and A. V. Zalygyn[a,b]

[a] *National Research Nuclear University "MEPhI", Moscow, 115409 Russia*
[b] *Shemyakin–Ovchinnikov Institute of Bioorganic Chemistry, RAS, Moscow, 117997 Russia*
**e-mail: belitskayakatya@yandex.ru*

Received February 21, 2023; revised February 26, 2023; accepted February 27, 2023.

Abstract—To date, the most common drug for diagnosis of cancer tumors is [^{18}F]-fluorodeoxyglucose, a radiopharmaceutical for positron emission tomography, which utilizes an increased glucose metabolism by cancer cells. At the same time, the approach based on glucose derivatives is not applicable in some cases. Inflammatory or other benign processes are often indistinguishable from tumors when the tumor is not specific to glucose, i.e., not only the malignant but also healthy cells actively consume [^{18}F]-fluorodeoxyglucose. In these cases, it is necessary to utilize other metabolic pathways, which can be specific to radiopharmaceuticals for a specific tumor in a given organ.

Keywords: radiopharmaceuticals, radiopharmacology, radiochemistry, PET, SPECT

DOI: 10.1134/S1068162023060043

CONTENTS

1. INTRODUCTION

Oncological diseases are becoming one of the general causes of death worldwide. A key element of successful cancer treatment is precise and timely diagnosis. Radiopharmaceuticals (RPPs) for positron emission tomography (PET) and single-photon emission computed tomography (SPECT) are tools for diagnosing and determining the stage of a tumor [1].

However, most radiopharmaceuticals are used to visualize glucose-specific tumors. Despite the high sensitivity and specificity, these drugs cannot always detect tumor cells, which do not need much glucose or are located in places with increased glucose consumption, e.g., in the brain. In these cases, the use of RPP in the diagnosis of tumor diseases is limited. To overcome this problem, researchers have been developing other metabolic pathways and compounds for tumors that are nonspecific to glucose. It is most preferable to classify these drugs specifically by targets for RPPs, i.e., chemical processes in tumors and involved compounds [2]. The classification of non-glucose-specific RPPs is given in Table 1.

Abbreviations: RPP, radiopharmaceutical preparation; PET, positron emission tomography; SPECT, single-photon emission computed tomography; FDG, fluorodeoxyglucose; FLT, 3′-deoxy-3′-^{18}F-fluorothymidine; FMT, fluoromethyltyrosine; CT, computed tomography; MRI, magnetic resonance imaging.

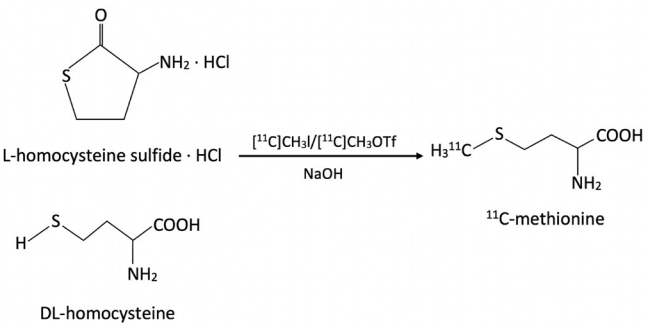

Fig. 1. Radiochemical synthesis of [^{11}C]-methionine. Adapted from Lodi et al. [3].

Among RPPs presented in Table 1, six drugs are the most studied and often used in the clinic, i.e., ^{11}C-methionine, ^{18}F-FLT, ^{11}C-choline, and ^{18}F-FMISO for PET diagnostics and ^{99m}Tc-annexin-V and ^{111}In-octreotide for SPECT studies.

Due to the widespread use of these drugs, they were chosen as examples for a more complete and detailed review of the clinical characteristics of RPPs used for the diagnosis of non-glucose-specific tumors.

2. SYNTHESIS OF RPP

The first stage in the creation of RPP is the radionuclide synthesis. Isotope ^{11}C is obtained, as a rule, on compact cyclotrons, which are installed directly in the hospital. The main reaction is the bombardment of nitrogen nuclei with protons (^{14}N(p,α)^{11}C). The half-life of the resulting isotope is ~20 min, which provides a low dose load for the patient and gives doctors the opportunity to repeat measurements. The radionuclide decay accompanied by the emission of positrons with a maximum energy of 0.961 MeV by 99.76% through the positron decay mode and by 0.24% according to the mechanism of electron capture. The positron decay leads to the formation of two annihilation quanta with the energy of 0.511 MeV, which are recorded by a tomography detector system.

The synthesis of ^{11}C-methionine is the ^{11}C-methylation of L-homocysteine sulfide-anion, which is obtained in the presence of the thiolactone bases, precursors of L-homocysteine. The reaction in Fig. 1 occurs at a high temperature, followed by purification to obtain a sterile solution of ^{11}C-methionine for clinical use [3].

^{11}C-choline is synthesized through the intermediate formation of ^{11}C-methyl iodide. First, [^{11}C]-CO_2 is reduced to methanol using $LiAlH_4$ in tetrahydrofuran (THF). After the evaporation of THF, a 57% solution of hydroiodic acid is added to the reaction mixture. The reaction of HJ with [^{11}C]–MeOH leads to the formation of [^{11}C]-CH_3I [4]. This product is transferred to another reaction vessel and dissolved in dimethylaminoethanol (0.5 mL) at –10°. The heating of the reaction mixture at 130°C for 5 min results in the formation of ^{11}C-choline. The reaction vessel is vacuumed at 130°C to remove the precursors, and the resulting product, ^{11}C-choline iodide, remains in the vessel. Then this product is dissolved in water and purified on a cartridge with cation exchange resin. The entire process of [^{11}C]-choline production takes 20 min. ^{11}C-choline (11 GBq or 300 mCi) is obtained from 26 GBq (700 mCi) [^{11}C]-CO_2. This drug is ready for medical use [5].

The ^{99m}Tc radionuclide is generated by the fission of ^{99}Mo for 6 h using a generator system (Fig. 2) [6]. This radioisotope is used for the preparation of ^{99m}Tc-annexin-V. Annexin-V is usually expressed in *E. coli* [7]. In one of the existing studies, glucoheptonate is used as an exchange agent for labeling with Tc. A solution that contained 20 mM sodium glucoheptonate in 10 mM HEPES buffer (4-(2-hydroxyethyl)-1-piperazine ethanesulfonic acid) (pH 6.6) is deoxygenated with argon,

Table 1. Classification of non-glucose-specific RPPs

Based on amino acids	To assess DNA synthesis	Based on lipids	To assess angiogenesis	To assess apoptosis	To assess hypoxia	Interacting with tumor receptors
^{11}C-methionone ^{18}F-FMT	^{11}C-thymidine ^{18}F-FLT	^{11}C-cholin ^{18}F-cholin ^{11}C-acetate	^{68}Ga-NOTA-RGD ^{18}F-galacto-RGD	^{99m}Tc-annexin-V ^{124}I-annexin-V	^{18}F-FMISO ^{18}F-FAZA ^{64}Cu-ATSM	With estrogen receptors: ^{18}F-fluoroestradiol With somatostatin receptor: ^{68}Ga-DOTA-TOC ^{111}In-octreotid ^{99m}Tc-TOC ^{99m}Tc-TATE

Note: FMT, dluoromethylthyrosine; FLT, 3′-deoxy-3′-^{18}F-fluorothymidine; NOTA, 1,4,7-troazacyclononane-*N*,*N*′,*N*″-triacetic acid; RGD, arginylglycylasparage acid; FMISO, fluoromisonidasole; FAZA, fluoroazomicyne arabinoside; ATSM, diacetyl-*bis*(*N*4-methylthiosemicarbazone); DOTA, tetraazamacrocyclic ligands; TOC, Tyr3-octreotide; TATE, Tyr3-octreotate.

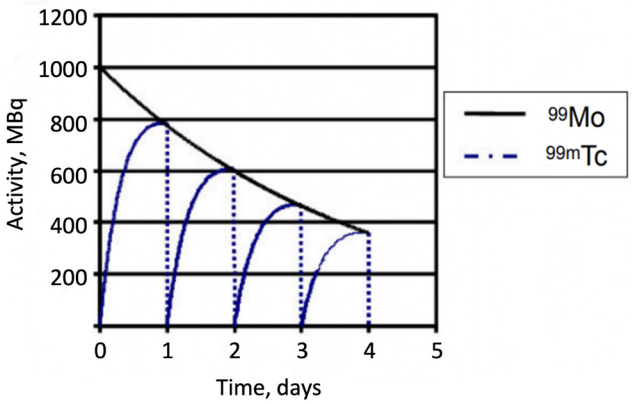

Fig. 2. Elution of $^{99}Mo/^{99m}Tc$ generator. Nominal activity of the generator is 1000 MBq at day 0 (Mobday). Elution every day, five times a week to obtain 1000, 780, 600, 470, and 360 MBq. Adapted from Bailey et al. [6].

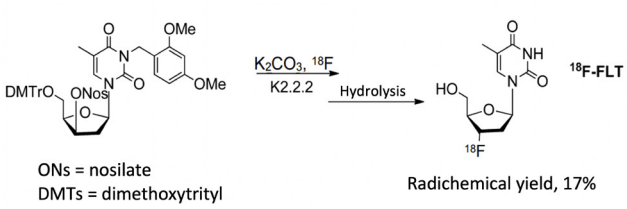

Fig. 3. Synthesis of ^{18}F-FLT. Adapted from Jacobson et al. [9].

Fig. 4. Chemical structure of (a) and ^{18}F-FMISO (b). Adapted from Lee et al. [25].

followed by the addition of $SnCl_2 \cdot 2H_2O$ up to 128 μg/mL. Aliquots of 1 mL are poured into borosilicate glass vials, lyophilized, closed under argon with screw caps with Teflon lining, and stored at –20°C. Using $SnCl_2$ as a reducing agent and glucoheptonate as an exchange agent, the protein can be labeled with ^{99m}Tc. For this purpose, $^{99m}TcO_4$ in 0.9% NaCl (100 μL) is added to tin/glucoheptonate (200 μL), followed by the addition of reduced protein (100 μg, 100 mL). The reaction mixture is incubated for 60 min at room temperature [8].

^{18}F is usually produced on a cyclotron by the proton irradiation of ^{18}O, a stable natural oxygen isotope. When the target is liquid $H_2{}^{18}O$, an aqueous solution of ^{18}F-fluoride ion is obtained. Nuclear characteristics of ^{18}F are the following: positron decay, 97% in most cases; half-life, ~110 min; emitted positron energy, 835 keV [9].

For the production of ^{18}F-FLT and ^{18}F-FMISO, the reaction of aliphatic nucleophilic fluorination is used, which involves the S_N2 substitution of a leaving group in precursors for ^{18}F-fluoride. The detailed synthesis of ^{18}F-FLT and ^{18}F-FMISO is shown in Figs. 3 and 4, respectively.

^{111}In, mainly in the form of indium chloride ($^{111}InCl$), is obtained on cyclotrons by irradiation of the cadmium target with a proton stream through either the $^{112}Cd(p,2n)^{111}In$ or $^{111}Cd(p,n)^{111}In$ reactions [10]. The first reaction is used more often because it leads to the radionuclide of a higher purity [10]. The main pollutant is a byproduct of the nuclear $^{114}m^2In$ reactions ($T_{1/2}$ = 49.51 days, Eγ = 190.3 keV, Iγ = 15.0%, IT 96.75%, EC 3.25%), which creates the 80 times higher absorbed dose than ^{111}In with the same activity. Nuclear characteristics of ^{111}In are the following: decay mode, electron capture (EC = 100%); half-life, 2.81 days; 7/2 → 5/2 transition energy, Eγ = 171.3 keV, Iγ = 90.3%; 5/2 → 1/2 transition energy, Eγ = 245.4 keV, Iγ = 94%.

$^{111}InCl$ is used to bind the radionuclide to antibodies, peptides, or other molecules using a chelate to firmly bind the ^{111}In ion to the octreotide peptide molecule through the covalent bonds. ^{111}In-pentetreotide is also produced in this way, i.e., octreotide binds to ^{111}In through diethylenetriamine pentaacetic acid (DTPA) [10].

3. BIODISTRIBUTION OF RPP

PET is used as a valuable diagnostic method for numerous pathologies. Various radiopharmaceuticals are involved in metabolic processes in different organs; therefore, their distribution in the body and affinity to different tissues are also distinguishable.

3.1. Biodistribution in Laboratory Animals

Several studies were performed to assess the biodistribution of ^{11}C-methionine in laboratory animals. The distribution of the drug in pigs was as follows. The highest concentration of ^{11}C-methionine was found in the small intestine, liver, kidneys, thymus, duodenum, and bones; lower activity of the drug was observed in other regions, such as the colon, heart, and brain; insignificant activity was detected in the bladder [11]. Similar results were obtained when studying the biodistribution of ^{11}C-methionine and ^{18}F-FDG preparations in intact Wistar rats [12]. The highest accumulation of the drugs was detected in the liver and spleen, whereas almost no drugs were observed in the brain and heart (Fig. 5).

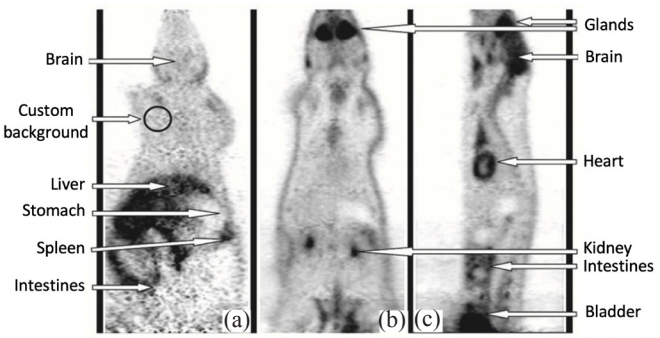

Fig. 5. Accumulation in a rat of ^{11}C-methionine (coronal view) (a) and ^{18}F-FDG (coronal and sagittal views) (b) and (c), respectively. Adapted from Stolc et al. [12].

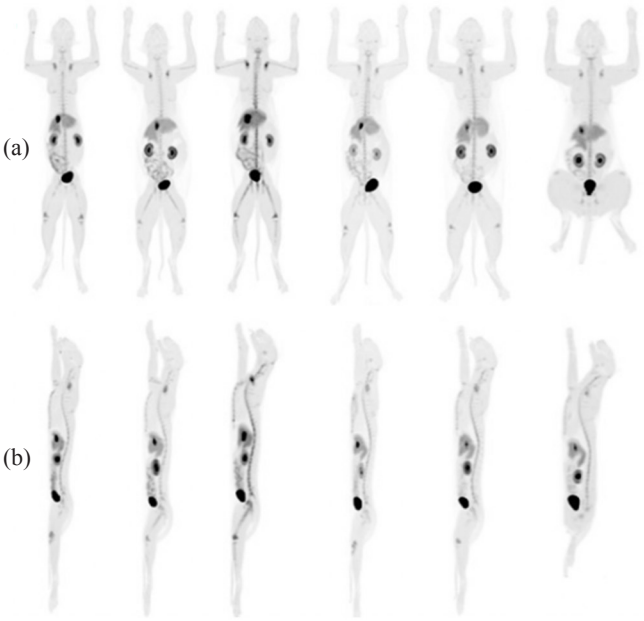

Fig. 6. Representative images of ^{18}F-FLT distribution throughout the body in healthy young adult cats 80.8 ± 7.5 min (mean = SD) after injection. Projections of the maximum PET intensity in the dorsal (a) and sagittal (b) planes are given. Adapted from Rowe et al. [14].

The biodistribution of ^{18}F-FLT in mice was studied in [13]. A significant amount of the drug was accumulated in the blood, plasma, liver, kidneys, and small intestine; a much lower concentration was observed in the brain, spinal cord, heart, and muscles. The biodistribution of ^{18}F-FLT was studied in adult domestic cats [14]. The highest absorption of the drug was detected in the intestine, the hepatobiliary system (a complex of organs and tissues related to the liver, gallbladder, and bile ducts), and urinary organs (Fig. 6). Minimal absorption was detected in the brain, lungs, myocardium, skeletal muscles, and spleen. Intensive accumulation in the urinary system is most likely due to the excretion of RPP through the kidneys.

Zheng et al. studied the biodistribution of ^{11}C-choline in mice with breast cancer atimia [15]. The absorption of the drug in tumors was 1.8–2.0%. The highest accumulation was observed in organs, such as the kidneys (15–24%), liver (7–13%), and small intestine (4–7%) (Fig. 7).

Tolvanen et al. [16] studied the distribution of ^{11}C-choline in laboratory rats (Fig. 8). Radioactivity was detected primarily in the kidneys, lungs, adrenal glands, and liver, whereas minimal accumulation was observed in the brain. The absorption of the radioactive drug in each of these organs gradually decreased 10 min after injection.

To assess the biodistribution of ^{99m}Tc-annexin-V, the drug was administered through the tail vein to laboratory mice [17]. The results of biodistribution were recorded 60 min after injection. The highest absorption was observed in the kidneys and liver. Blankenburg et al. [18] also studied the biodistribution of ^{99m}Tc-annexin-V in mice. The authors showed that the lowest accumulation (less than 0.2% of the administered dose) was recorded in the brain, heart, and thymus. The researchers noticed that the drug was localized in the kidneys, mainly in the renal cortex. The drug was also found in other organs, such as the spleen, stomach, and lungs.

The biodistribution of ^{18}F-FMISO was studied in mice with bowel cancer [19]. The authors showed an increased accumulation of ^{18}F-FMISO in healthy intestinal and liver and observed this drug in mouse tumors of other organs (Fig. 9). This fact can be explained by the large number of RPP-absorbing anaerobic bacteria in the intestine and the lipophilicity of ^{18}F-FMISO described above. The lowest content of this RPP was observed in the blood, spleen, heart, stomach, and especially the muscles 120 min after administration; a slightly higher content was found in the lungs and bones. The tumor showed approximately the same absorption as the kidneys but ~2 times less than the intestine and 1.5 times less than the liver.

The biodistribution of ^{111}In-octreotide in rats and mice was investigated using plasma-substituting drugs in [20]. Plasma substitutes have been used because ^{111}In-pentetreotide, due to its peptide nature, usually demonstrates increased renal absorption, which limits the administered dose of this RPP. Adjusted for the use of plasma substitutes (PBS, lysine, and gelofusine) in the case

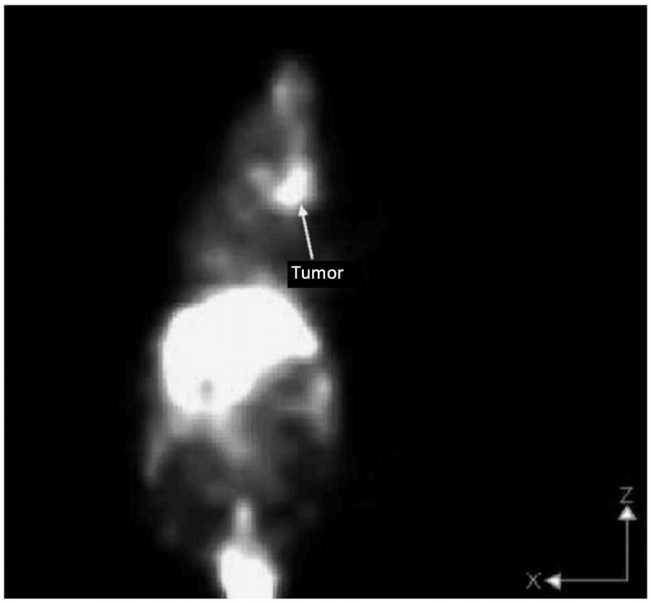

Fig. 7. Visualization of ^{11}C-choline distribution in a mouse with MCF-7 atimia (Michigan Cancer Foundation-7), which was transfected with implanted IL-lα. Adapted from Zheng et al. [15].

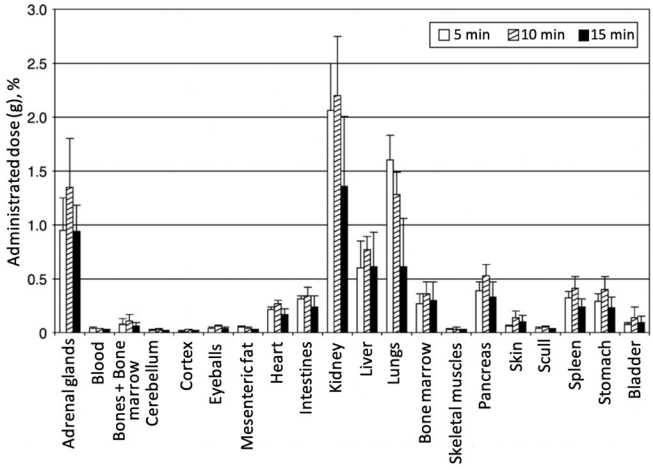

Fig. 8. Adsorption of radioactivity in different organs 5, 10, and 15 min after injection of ^{11}C-choline. To determine the absorption in the organs, three rats were used at a specified period of time, and two rats were used for blood, cerebellum, and cerebral cortex. Adapted from Tolvanen et al. [16].

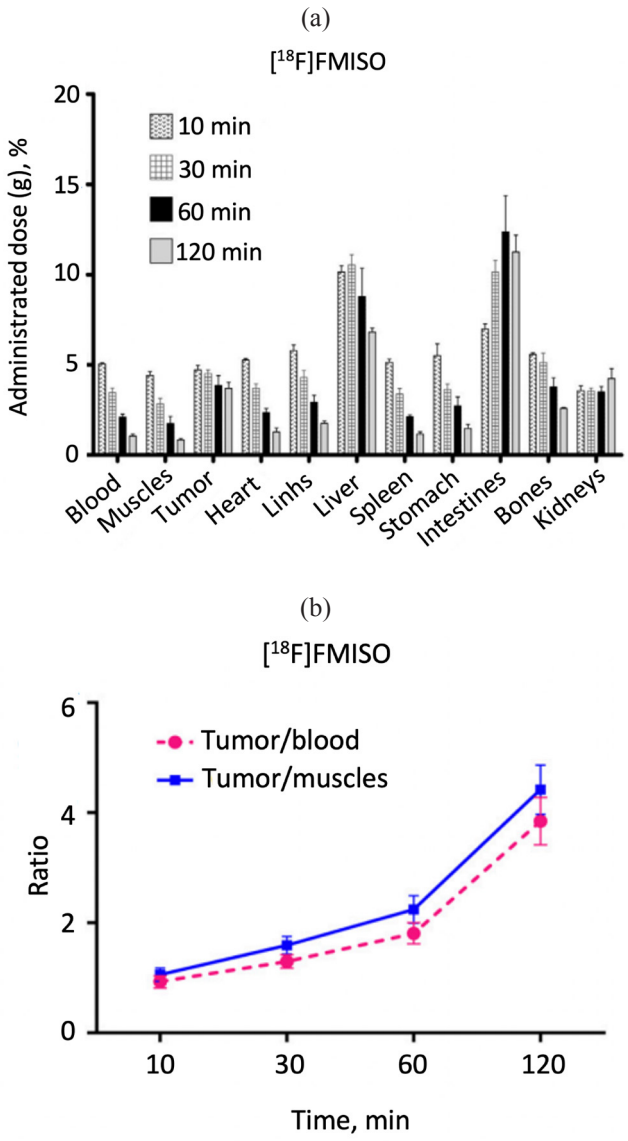

Fig. 9. Biodistribution of ^{18}F-FMISO (0.15 MBq/mL) in xenotransplanted mice CT-26 10, 30, 60, and 120 min after injection (a); the ratio of tumor to blood and tumor to muscle at a specified period of time, (b). The results represent the average percentage of the administered dose per 1 g of tissue ± standard deviation (%ID/г ± SD); $n = 4$ at each time. Adapted from Seelam et al. [19].

of rats, the results showed very low adsorption in organs and tissues, such as liver, spleen, lungs, intestines, muscles, and blood but very high adsorption in the adrenal glands, pancreas, and kidneys (Fig. 10). Biodistribution of ^{111}In-octreotide in mice with the same plasma substitutes showed different results, i.e., an increased accumulation in the lungs but decreased (compared to rats) accumulation in receptor-positive organs, such as the adrenal glands and pancreas.

3.2. Biodistribution in Humans

Harris et al. studied the biodistribution of ^{11}C-methionine in non-tumor organs in children, who were examined for malignant diseases [21]. The highest content of ^{11}C-methionine was found in the pancreas and

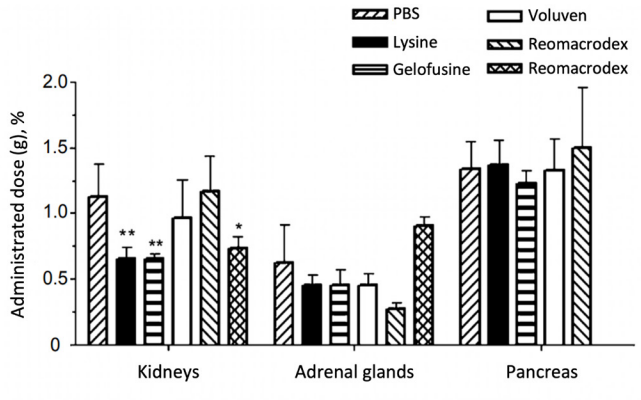

Fig. 10. Biodistribution data obtained with the use of various plasma expanders 20 h after intravenous administration of ^{111}In-octreotide to rats. Rats were intravenously injected with PBS, lysine (80 mg), gelofusine (20 mg), voluven (20 mg), reomacrodex (30 mg), or hemaxel (17.5 mg) (0.5 mL) 2–5 min before administration of ^{111}In-octreotide. The results are presented as an average of % ID/g; error bars indicate SD. *, $p < 0.05$; **, $p < 0.01$. Adapted from Van Eerd et al. [20].

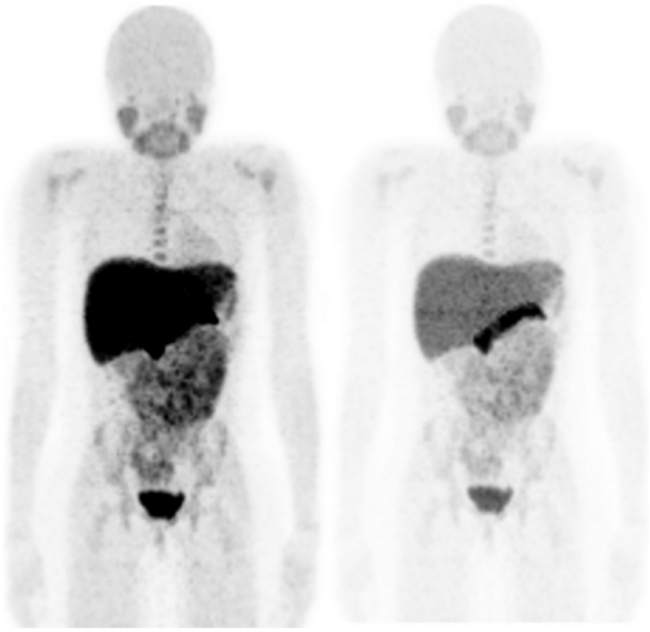

Fig. 11. A projection image of the front part of the body with maximum intensity in a 7-year-old girl examined for brain neoplasms. Two images with different intensities show the relative distribution of ^{11}C-methionine [21].

liver (Fig. 11). Less intense absorption was observed in other organs, such as the salivary glands, tonsils, and bone marrow. Absorption was negligible in the lungs, adipose tissue, and muscles. Accumulation in the bone marrow, parotid glands, and tonsils was insignificant; however, it was statistically significantly higher in men than women. The high content of ^{11}C-methionine was reliably detected in the pancreas and liver, which is consistent with the anabolic functions of these organs. Intensive absorption in the upper abdomen may limit the diagnostic usefulness of ^{11}C-methionine in this area.

The pharmacokinetics and dosimetry of ^{11}C-methionine in adults are described by Dela et al. based on the PET data of the whole body [22]. The pancreas, liver, bladder, and kidneys showed the highest initial absorption of ^{11}C-methionine. Patients in this study were scanned at several points in time to calculate doses. The pancreas and liver had the highest activity among the studied organs.

The first studies of biodistribution of ^{18}F-FLT in humans showed physiological uptake in the bone marrow, liver, and urinary tract. Absorption is not observed in the brain, skeletal muscles, and myocardium. The distribution of this RPP in the human body (Fig. 12) showed an increased absorption of ^{18}F-FLT in the bone marrow, liver, and spleen [23].

Tolvanen et al. [16] studied the distribution of ^{11}C-choline in humans. The drug primarily accumulated in the renal cortex, salivary glands, liver, spleen, pancreas, blood, and muscles (Fig. 13). Particular attention was paid to the evaluation of the RPP dose in the bones because the bone marrow is very sensitive to radiation. The results of PET studies did not demonstrate the possibility of visualizing bone structures.

To assess the safety of ^{99m}Tc-annexin-V, Kemerink et al. studied its biodistribution in six male volunteers (Fig. 14) [24]. The results showed that kidneys, liver, red bone marrow, and spleen accumulated ~50, 13, 9.2, and 4.6% of the administered dose, respectively, 3 h after injection. The biological half-life of the drug recorded throughout the body was long (69.7 h). The absorbed doses were found to be 196 ± 31 Gy/MBc for the kidneys, 41 ± 12 Gy/MBc for the spleen, 16.9 ± 1.3 Gy/MBc for the liver, and 8.4 ± 0.9 Gy/MBc for red bone marrow. No side effects were observed.

The results of PET studies in humans using ^{18}F-FMISO are described in the review of Lee et al. [25]. The authors showed maximum absorption in the bladder (due to high absorption in urine) and high absorption in the intestines, liver, and kidneys. The lowest absorption was detected in organs and tissues, such as blood, spleen, heart, lungs, muscles, bones, and brain.

The study of the biodistribution of ^{111}In-octreotide in the human body provides valuable information about its

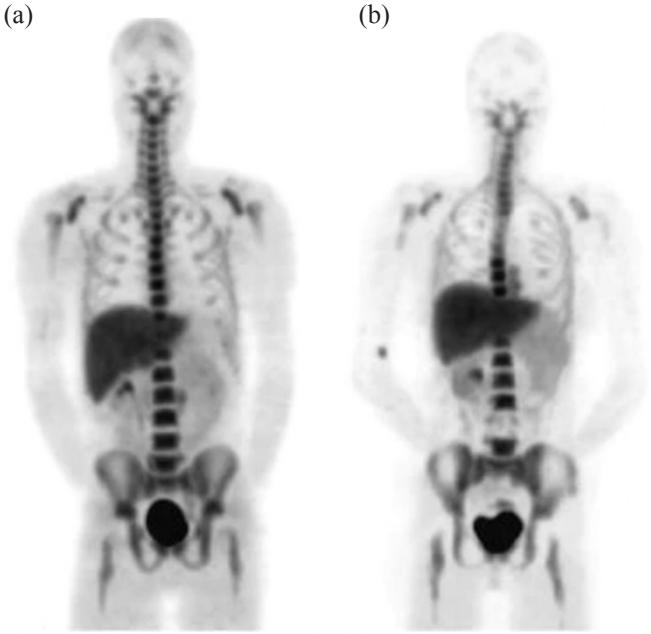

Fig. 12. The normal distribution of ^{18}F-FLT detected by PET. The effect of radiation therapy on bone marrow activity in the fourth lumbar vertebra (a) and middle thoracic vertebrae (b). Adapted from Agool et al. [23].

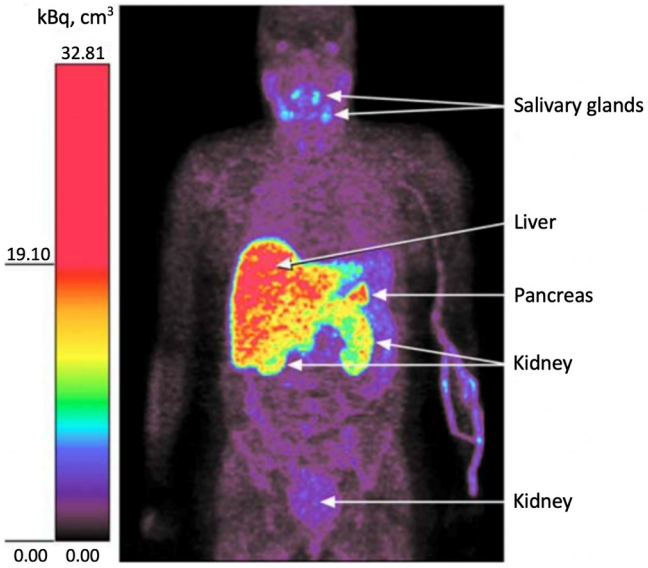

Fig. 13. Representative coronal PET image of the entire body of a patient with rheumatoid arthritis 10 min after injection of ^{11}C-choline. Adapted from Tolvanen et al. [16].

localization in tissues. In healthy people, relatively high absorption of this drug is observed in the spleen, liver, kidneys, and bladder. Weak absorption may also occur in the pituitary, thyroid, and salivary glands. When using the drug, there is usually visible intestinal activity, which mainly increases on delayed images. The radioactivity

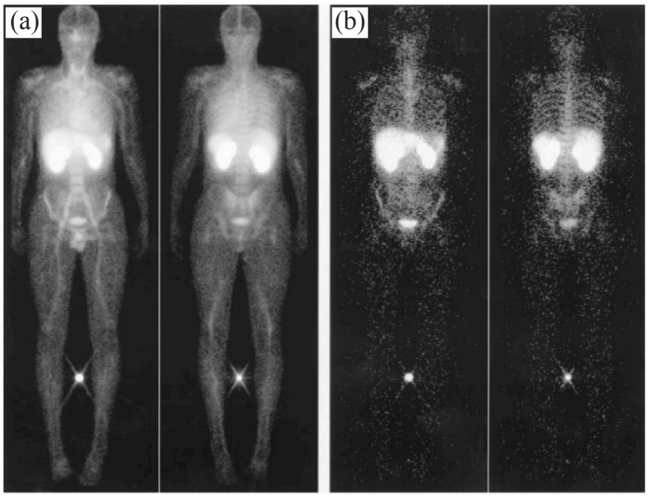

Fig. 14. Conjugated images of the entire body of a 22-year-old male volunteer 30 min (a) and 24 h (b) after intravenous injection of ^{99m}Tc-annexin-V. Adapted from Kemerink et al. [24].

in the cardiovascular blood flow is usually visible on early images. Thus, delayed images are more useful for assessment of mediastinal lesions (pathological conditions that capture the mediastinal region, i.e., the space between the sternum and the spine, where the organs of the thoracic cavity are located) [26]. Forssell-Aronsson et al. [27] studied the biodistribution of intravenously administered [^{111}In-DTPA-Phe1]–octreotide in 100 patients. Among tumor tissues, the highest activity (0.33–77% IA/kg) was found in carcinoid tumors. The absorption values in medullary thyroid carcinoma and differentiated thyroid tumors were 0.017–7.8 and 0.061–88% IA/kg, respectively. Interestingly, no differences were found in this study in the absorption of octreotide by benign and malignant tumors. At the same time, two metastases of lymph nodes of one of the Hurthle cell carcinomas of the thyroid gland showed very high absorption values (40 and 88% IA/kg, respectively). In the case of breast cancer, the highest activity of ^{111}In was 0.61–7% IA/kg. Very high activity of ^{111}In was detected in all endocrine pancreatic tumors (EPT), except for one case of insulinoma. In general, the highest activity of ^{111}In was recorded mainly in metastases (and not in primary tumors), which was observed in the cases of lymph node and liver metastases, although there were several exceptions.

4. TARGET FOR RPP

Tumor cells differ from healthy tissues in not only their instability and rapid division but also their ability to

accumulate RPP. This property makes it possible to use RPP in the diagnostics and treatment of various types of cancer. However, it is necessary to choose the accurate target for RPP to achieve maximum effectiveness of the treatment. In this section, we will consider targets for the RPP delivery to cancer tissues and the effect of target selection on the efficacy of the treatment.

Methionine is an essential amino acid necessary for cell growth and replication. As cells replicate, the need for protein and phospholipid synthesis increases, which makes the transport and regeneration of essential amino acids critically important for tumor growth. It is known that facilitated amino acid transport is enhanced through glioma capillaries, and tumors can stimulate increased expression of amino acid transporters in their supportive vascular network [28]. The dependence on methionine may reflect a general imbalance in transmethylation, which leads to hypermethylation of some substances and hypomethylation of others in tumor cells.

^{18}F-FLT penetrates the cell through both passive diffusion and facilitated transport by Na^+-dependent carriers. Subsequently, ^{18}F-FLT is phosphorylated by thymidine kinase 1 (TK1) into ^{18}F-FLT monophosphate, which is retained in the cell [29]. It has been found that TK1 is one of the markers of proliferating cells, which can be used in the assessment of a cancerous tumor [30]. Thus, it was found that the activity of TK1 in malignant cells is higher than in benign cells by factors of 3–4, which contributes to a higher accumulation of ^{18}F-FLT in tumor cells compared to healthy tissue.

The tumor formation leads to an increase in the level of intracellular phosphorylcholine, which is a key intermediate in the synthesis of phosphatidylcholine. That is why, rapidly proliferating tumor cells contain a high content of phosphatidylcholine and other phospholipids. Administrated ^{11}C-choline is transferred to these cells by specific transporters; it can also be absorbed through the blood-brain barrier and cell membrane [31].

One of the signs of the onset of cell apoptosis is the formation of phosphatidylserine on the cell surface. Phosphatidylserine is a simple anionic phospholipid, which is usually confined to the inner sheet of the plasma membrane. Annexin-V has a high affinity for phosphatidylserine-bound cell membranes; therefore, this preparation is used to detect apoptosis in hematopoietic cells, neurons, fibroblasts, endothelial cells, smooth muscle cells, carcinomas, and lymphomas. This protein has also been proposed by Stratton et al. [32] as an imaging tool for detecting blood clots *in vivo* because activated platelets express a large amount of phosphatidylserine on their surface.

^{18}F-FMISO is a biological marker of tissue hypoxia. The process of accumulation of ^{18}F-fluoromizonidazole in poorly oxygenated tissues is described in detail by Lee et al. [25]. ^{18}F-FMISO enters the cell by passive diffusion and is reduced there with nitroreductase enzymes, after which it can be preserved within the cell only under reduced partial pressure of oxygen in the tissue. In normally oxygenated tissues, the parent compound (unmetabolized form of RPP, ^{18}F-FMISO) is rapidly reoxygenated with excess oxygen and does not remain in the cells of these tissues. It follows that there is an inverse correlation between the accumulation of RPP and the oxygen content in a particular tissue. At the same time, a critical condition for preservation of ^{18}F-FMISO in the cell is the presence of functioning reductases, which are inactive in necrotic tissues. Thus, the target for this RPP can be all pathologies, which lead to a reduced supply of oxygen to the tissue (but not necrosis).

Octapeptide octreotide is an analog of the natural hormone somatostatin; therefore, it binds to tumor cells with somatostatin receptors [33].

5. APPLICATION OF PFT IN THE DIAGNOSIS OF DISEASES

The use of various RPPs differs depending on different pathologies. This section provides examples of using RPPs as compounds for the diagnosis of certain diseases.

^{11}C-methionine is mainly used in the diagnosis of focal lesions in the central nervous system. This radiopharmaceutical is also used in some studies for the diagnosis of multiple myeloma and primary, secondary, and tertiary hyperparathyroidism. ^{11}C-methionine can be used also for the diagnosis of lymphoproliferative diseases and solid tumors.

^{18}F-FLT is a PET indicator, which is increasingly used in PET/CT studies to assess the oncological response because it is a biomarker of tumor proliferation for several types of cancer, such as NSCLC (non-small cell lung cancer), squamous cell head and neck cancer, and breast cancer.

^{11}C-choline is used in PET diagnostics to detect diseases, such as prostate, esophagus, bladder, and brain tumors. In some studies, this drug was used to visualize

synovial proliferation associated with rheumatoid arthritis.

The imaging of labeled annexin-V is being developed for use in oncology, organ transplantation, and therapy of cardiovascular diseases. In particular, this drug makes it possible to visualize apoptotic cells in acute myocardial infarction, myocarditis, rejection of a heart transplant, unstable atherosclerotic plaque, and tumors after effective chemotherapy. It is noteworthy that ^{99m}Tc-annexin-V was used to monitor the therapeutic effect of anti-apoptotic drugs in patients with heart failure [34].

^{18}F-FMISO is a biomarker of tissue hypoxia, which is characteristic of solid tumors. The application of this compound is described for the diagnosis of head and neck tumors and squamous cell carcinoma (skin cancer) [35]. The use of ^{18}F-FMISO in the diagnosis of soft tissue sarcomas was also successful [36].

As mentioned above, octreotide reacts with somatostatin receptors, thus visualizing all pathological processes, which provide the expression of somatostatin receptors [37], i.e., tumors with a high level of receptor expression, tumors of the sympathoadrenal system (pheochromocytoma, neuroblastoma, ganglioneuroma, and paraganglioma), gastroenteropancreatic tumors (GEO), small cell lung cancer, breast cancer, lymphomas, astrocytomas, etc.

^{11}C-methionine is primarily used in clinical studies for the diagnosis of various brain diseases (gliomas and glioblastomas). There is a review of studies, which evaluate the accuracy of PET with ^{11}C-methionine in the detection of brain glioma and metastases [38]. It was found that an accuracy of 76–100% was achieved in both low- and high-grade gliomas. However, it was concluded that PET with ^{11}C-methionine does not allow one to assess the degree of malignancy of glioma. Nineteen people with the detected multiple myeloma were examined to evaluate the accuracy of using ^{11}C-methionine to diagnose this disease [39]. PAT/CT with ^{11}C-methionine revealed active multiple myeloma in 15 (78.9%) out of 19 patients, and a disseminated (widespread) form of the disease was detected in 7 (36.8%) out of 19 individuals.

The overview of recent PET studies using ^{18}F-FLT was analyzed to assess the diagnostic efficacy of this method [29]. RPP showed 86% accumulation in malignant tissues in the study of small-cell lung cancer, and there was no detection in benign tissues, which indicates 100% specificity of this drug. The diagnosis of the chest tumors showed the following results. The drug demonstrated 56% accuracy in the detection of malignant formations, and its specificity was 100%. In the study of brain tumors, ^{18}F-FLT showed insufficient characteristics and limited visualization ability. However, this RPP was more specific in the detection of relapses compared to ^{18}F-FDG. In general, it is not entirely clear whether ^{18}F-FLT can be quite specific to distinguish healthy tissue from malignant tissue in the brain. In the study of colorectal cancer, ^{18}F-FLT showed high sensitivity (>90%) with a specificity of 76%. ^{18}F-FLT was able to differentiate between low-grade and high-grade soft tissue sarcoma according to the classification system. However, it was impossible to distinguish between benign and low-grade malignant soft tissue tumors.

Lapa et al. [39] studied the effectiveness of ^{11}C-choline for the diagnosis of multiple myeloma. In these experiments, ^{11}C-choline was used along with ^{11}C-methionine on 19 patients. PET/CT with ^{11}C-choline showed a positive result in 14 (73.7%). In the remaining four patients (21.1%), metabolically active myeloma could not be detected. As for intramedullary lesions of multiple myeloma, PET/CT with ^{11}C-choline revealed a lesion of the appendicular skeleton in 11 (57.9%) out of 19 patients.

^{11}C-choline is used to monitor patients with prostate cancer. Krause et al. [40] performed ^{11}C-choline-PET/CT study on 63 patients with prostate cancer with biochemical recurrence after primary therapy. The authors revealed a significant and strict correlation between the detection rate of cancer and the level of the serum prostate-specific antigen (PSA). The detection rates were 36, 43, 62, and 73% at the PSA concentration of <1, 1–2, 2–3, and ≥3 ng/mL, respectively. The overall detection rate of prostate cancer using ^{11}C-choline-PET/CT was 59%.

One of the alternative methods of labeling annexin-V is the use of ^{99m}Tc–hydrazinonicotinamide-annexin-V (^{9m}Tc-HYNIC-annexin-V). Thismuch modification provides a much simpler and faster preparation of this drug with significantly higher radiochemical yields at room temperature and requires much lower initial radioactivity values (1.11–1.48 GBq). All these advantages make ^{99m}Tc-HYNIC-annexin-V a much more suitable drug for routine production and clinical use compared to other methods of labeling annexin-V. A study of 18 patients with head and neck cancer showed a high correlation between the quantitative uptake of ^{99m}Tc-annexin-V by the tumor and the number of apoptotic tumor cells. However, the average percentage of absolute absorption of the administered dose per 1 cm^3

of the tumor was only 0.0003% 1 h after injection and 0.0001% after 5–6 h of injection ($p = 0.012$) [41]. Narula et al. [42] described the use of ^{99m}Tc-annexin-V to visualize apoptosis in the rejection of a cardiac allograft. In the study with 18 cardiac allograft recipients, five patients had positive myocardial uptake of ^{99m}Tc-annexin-V, and 13 patients had no uptake.

Hirata et al. [43] performed PET studies of class IV glioma using ^{18}F-FMISO and showed 100% sensitivity and 100% specificity. At the same time, a comparative study of using ^{18}F-FDG for the same tumors showed only 66% specificity with the same sensitivity.

According to the study by Shi et al. [44], ^{111}In-octreotide scintigraphy proved useful in determining both primary tumors and distant metastases for the majority of patients ($n = 48$). In this study, octreotide scintigraphy showed 95% sensitivity for carcinoids, while the sensitivity of PET measurements was only 90.6%, which corresponded to the range of sensitivity values of ^{111}In-octreotide (85–95%). Among all 83 tumor lesions, 33 (44%) were detected by CT, 29 (43%) by MRI, and 72 (87%) by the Osteoscan procedure (^{111}In-octreotide scintigraphy). At the same time, unlike MRI, the detection rate of bone carcinoid metastases was low in the latter study (30%). Rubello et al. [26] demonstrated high sensitivity of ^{111}In-octreotide scintigraphy in detecting pheochromocytoma (86%), paraganglioma (100%), and neuroblastoma (89%). However, a malignant neoplasm of the adrenal glands may be hidden by the presence of intense kidney activity. Moreover, ^{111}In-octreotide is not a specific indicator of symphatomedullary tumors because of a significant absorption in most other neuroendocrine benign and malignant tumors, some nonendocrine tumors, granulomatous diseases, and autoimmune disorders.

This absorption is associated with a wide spread of cells (including activated lymphocytes) throughout the body, which express somatostatin receptors on their surface. Thus, it seems reasonable to consider scintigraphy with ^{111}In-octreotide as the second choice method for sympathomedullary imaging after metaiodobenzylguandine (MIBG) scintigraphy especially when the result of the MIBG analysis is completely or partially false negative. Conversely, scintigraphy with ^{111}In-octreotide, due to its high sensitivity, can be considered a first-choice scintigraphic imaging method for neuroendocrine tumors, such as carcinoids, pituitary tumors, and pancreatic and gastrointestinal amine precursors. An extensive meta-analysis by Hoefnagel showed that ^{111}In-octreotide scintigraphy of 451 carcinoid patients had a sensitivity of 86%, while the sensitivity was 70% in a group of 275 patients receiving ^{131}I-MIBG. Thus, ^{111}In-octreotide is characterized by a very high sensitivity, which is confirmed by numerous studies. However, the specificity of this RPP is not high enough because of the wide prevalence of somatostatin receptors, which are expressed in tumor and healthy cells.

6. CONCLUSIONS

PET and SPECT are promising methods for the diagnosis of malignant neoplasms, which not only allow images of the tumor but also represent a new tool for the noninvasive study of the biology of the tumor. To date, clinicians mainly use RPPs aimed at glucose metabolism. However, some metabolically active tissues, such as myocardium, brain tissue, inflammation areas, and some benign tumors, may also show increased absorption of imaging agents, which leads to their low specificity. The use of RPPs based on other markers will increase the accuracy and specificity of diagnosis.

^{11}C-methionine is a promising PET-RPP. In recent years, more and more studies have been appearing, which are aimed at diagnosing and predicting brain tumors using ^{11}C-methionine.

^{18}F-FLT shows high results in modern research; it turns out to be the more reliable RPP compared to common ^{18}F-FDG for some types of cancer. Due to its properties, ^{18}F-FLT has 100% specificity and allows one to detect tissue proliferation in the brain.

^{11}C-choline accumulates directly in tumor cells, which ensures high accuracy in the diagnosis of metastases of all types. To date, many studies of ^{11}C-choline are devoted to the visualization of prostate cancer because this drug is most effective for this type of disease.

^{99m}Tc-Annexin-V is an inexpensive and available drug. Its short half-life (6 h) is optimal for the SPECT imaging of small molecules, peptides, and small proteins. In addition, low decay energy (0.14 MeV) of this drug provides low radiation doses for patients. Taken together, these desirable characteristics have led to the appearance of many studies of ^{99m}Tc-Annexin-V for the detection of apoptosis.

^{18F}-FMISO is the most widely used and validated PET–RPP for noninvasive assessment of hypoxia, which is gaining increasing importance due to its potential to predict the response to the treatment and provide forecasts for a wide spectrum of pathological processes.

^{111}In-DTPA-octreotide is the most common RPP for SPECT, which allows a high accuracy and specificity in the diagnosis of a wide range of tumor diseases with both high and low expression of somatostatin receptors.

FUNDING

The work was supported by the Russian Science Foundation (grant no. 23-24-10046).

ETHICS APPROVAL AND CONSENT TO PARTICIPATE

This article does not contain any studies conducted by any authors of this work. This article does not contain any studies involving patients or animals as test objects.

CONFLICT OF INTEREST

No conflict of interest was declared by the authors.

AUTHOR CONTRIBUTION

The authors EDB, VAD, and ANK—collected and analyzed the literature data and prepared the initial version of this review. Author AVZ—provided the financial support. Authors VAO and AVZ—conducted the organization of the process of writing this review. Authors EDB, VAD, and AVZ—analyzed the collected literature data, edited, and prepared the article for publication. The final variation of this review was approved by all of the authors.

DATA AVAILABILITY

The data that support the findings of this study are available from the corresponding author upon reasonable request.

REFERENCES

1. Wadsack, W. and Mitterhauser, M., *Eur. J. Radiology*, 2010, vol. 73, pp. 461–469. https://doi.org/10.1016/j.ejrad.2009.12.022
2. Lee, Y.S., *Open Nuclear Med. J.*, 2010, vol. 2, pp. 178–185. https://doi.org/10.2174/1876388X01002010178
3. Lodi, F., Malizia, C., Castellucci, P., Cicoria, G., Fanti, S., and Boschi, S., *Nuclear Med. Biol.*, 2012, vol. 39, pp. 447–460. https://doi.org/10.1016/j.nucmedbio.2011.10.016
4. Szydło, M., Jadwiński, M., Chmura, A., Gorczewski, K., and Sokół, M., *Contemp. Oncol. (Pozn)*, 2016, vol. 20, pp. 229–236. https://doi.org/10.5114/wo.2016.61566
5. Hara, T. and Yuasa, M., *Appl. Radiat. Isot.*, 1999, vol. 50, pp. 531–533. https://doi.org/10.1016/S0969-8043(98)00097-9
6. Bailey, D., Humm, J., Todd-Pokropek, A., and van Aswegen, A., *Nuclear Medicine Physics. A Handbook for Teachers and Students.* Vienna: International Atomic Energy Agency, 2014.
7. Wood, B.L., Gibson, D.F., and Tait, J.F., *Blood*, 1996, vol. 88, pp. 1873–1880. https://doi.org/10.1182/blood.V88.5.1873.1873
8. Tait, J.F., Brown, D.S., Gibson, D.F., Blankenberg, F.G., and Strauss, H.W., *Bioconjug. Chem.*, 2000, vol. 11, pp. 918–925. https://doi.org/10.1021/bc000059v
9. Jacobson, O., Kiesewetter, D.O., and Chen, X., *Bioconjug. Chem.*, 2015, vol. 26, pp. 1–18. https://doi.org/10.1021/bc500475e
10. Hermanne, A., Adam-Rebele, R., van den Winkel, P., Tárkányi, F., and Takács, S., *Radiochim. Acta*, 2014, vol. 102, pp. 1111–1126. https://doi.org/10.1515/ract-2013-2233
11. Afzelius, P., Nielsen, O.L., Alstrup, A.K., Bender, D., Leifsson, P.S., Jensen, S.B., and Schønheyder, H.C., *Am. J. Nuclear Med. Mol. Imaging*, 2016, vol. 6, p. 42.
12. Stolc, S., Jakubíková, L., and Kukurová, I., *Interdiscip. Toxicol.*, 2011, vol. 4, pp. 52–55. https://doi.org/10.2478/v10102-011-0010-1
13. Barthel, H., Cleij, M.C., Collingridge, D.R., Hutchinson, O.C., Osman, S., He, Q., Luthra, S.K., Brady, F., Price, P.M., and Aboagye, E.O., *Cancer Res.*, 2003, vol. 63, pp. 3791–3798.
14. Rowe, J.A., Morandi, F., Wall, J.S., Akula, M., Kennel, S.J., Osborne, D., Martin, E.B., Galyon, G.D., Long, M.J., Stuckey, A.C., and LeBlanc, A.K., *Veterinary Radiol. Ultrasound*, 2013, vol. 54, pp. 299–306. https://doi.org/10.1111/vru.12024
15. Zheng, Q.H., Stone, K.L., Mock, B.H., Miller, K.D., Fei, X., Liu, X., Wang, J.Q., Glick-Wilson, B.E., Sledge, G.W., and Hutchins, G.D., *Nuclear Med. Biol.*, 2002, vol. 29, pp. 803–807. https://doi.org/10.1016/s0969-8051(02)00339-6
16. Tolvanen, T., Yli-Kerttula, T., Ujula, T., Autio, A., Lehikoinen, P., Minn, H., and Roivainen, A., *Eur. J. Nuclear Med. Mol. Imaging*, 2010, vol. 37, pp. 874–883. https://doi.org/10.1007/s00259-009-1346-z

17. Tait, J.F., Brown, D.S., Gibson, D.F., Blankenberg, F.G., and Strauss, H.W., *Bioconjug. Chem.*, 2000, vol. 11, pp. 918–925. https://doi.org/10.1021/bc000059v
18. Blankenberg, F.G., Katsikis, P.D., Tait, J.F., Davis, R.E., Naumovski, L., Ohtsuki, K., Kopiwoda, S., Abrams, M.J., and Strauss, H.W., *J. Nuclear Med.*, 1999, vol. 40, pp. 184–191.
19. Seelam, S.R., Lee, J.Y., Kim, Y.J., Lee, Y.-S., and Jeong, J.M., *J. Radiopharm. Mol. Probes*, 2015, vol. 1, pp. 137–144. https://doi.org/10.22643/JRMP.2015.1.2.137
20. van Eerd, J.E.M., Vegt, E., Wetzels, J.F.M., Russel, F.G.M., Masereeuw, R., Corstens, F.H.M., Oyen, W.J.G., and Boerman, O.C., *J. Nuclear Med.*, 2006, vol. 47, pp. 528–533.
21. Harris, S.M., Davis, J.C., Snyder, S.E., Butch, E.R., Vāvere, A.L., Kocak, M., and Shulkin, B.L., *J. Nuclear Med.*, 2013, vol. 54, pp. 1902–1908. https://doi.org/10.2967/jnumed.112.118125
22. Deloar, H.M., Fujiwara, T., Nakamura, T., Itoh, M., Imai, D., Miyake, M., and Watanuki, S., *Eur. J. Nuclear Med.*, 1998, vol. 25, pp. 629–633. https://doi.org/10.1007/s002590050265
23. Agool, A., Glaudemans, A.W.J.M., Boersma, H.H., Dierckx, R.A.J.O., Edo Vellenga, E., and Slart, R.H.J.A, *Eur. J. Nuclear Med. Mol. Imaging*, 2011, vol. 38, pp. 166–178. https://doi.org/10.1007/s00259-010-1531-0
24. Kemerink, G.J., Liu, X., Kieffer, D., Ceyssens, S., Mortelmans, L., Verbruggen, A.M, Steinmetz, N.D., Vanderheyden, J.-L., Green, A.M., and Verbeke, K., *J. Nuclear Med.*, 2003, vol. 44, pp. 947–952.
25. Lee, S.T. and Scott, A.M., *Semin. Nucl. Med.*, 2007, vol. 37, pp. 451–461. https://doi.org/10.1053/j.semnuclmed.2007.07.001
26. Rubello, D., Bui, C., Casara, D., Gross, M.D., Fig, L.M., and Shapiro, B., *Eur. J. Endocrinol.*, 2002, vol. 147, pp. 13–28. https://doi.org/10.1530/eje.0.1470013
27. Forssell-Aronsson, E., Bernhardt, P., Nilsson, O., Tisell, L.-E., Wängberg, B., and Ahlman, H., *Acta Oncol.*, 2004, vol. 43, pp. 436–442. https://doi.org/10.1080/02841860410030670
28. Singhal, T., Narayanan, T.K., Jain, V., Mukherjee, J., and Mantil, J., *Mol. Imaging Biol.*, 2008, vol. 10, pp. 1–18. https://doi.org/10.1007/s11307-007-0115-2
29. Been, L.B., Suurmeijer, A.J.H., Cobben, D.C.P., Jager, P.L., Hoekstra, H.J., and Elsinga, P.H., *Eur. J. Nucl. Med. Mol. Imaging*, 2004, vol. 31, pp. 1659–1672. https://doi.org/10.1007/s00259-004-1687-6
30. Sergeeva, N.S., Parilova, N.K., Marshutina, N.V., and Meisner, I.S.., *Adv. Mol. Onkol.*, 2017, vol. 4, pp. 17–23. https://doi.org/10.17650/2313-805X-2017-4-1-17-23
31. Cornford, E.M., Braun, L.D., and Oldendorf, W.H., *J. Neurochem.*, 1978, vol. 30, pp. 299–308. https://doi.org/10.1111/j.1471-4159.1978.tb06530.x
32. Stratton, J.R., Dewhurst, T.A., Kasina, S., Reno, J.M., Cerqueira, M.D., Baskin, D.G., and Tait, J.F., *Circulation*, 1995, vol. 92, pp. 3113–3121. https://doi.org/10.1161/01.cir.92.10.3113
33. Dedov, I.I. and Vaks, V.V., *Problems Endocrinol.*, 2004, vol. 50, pp. 42–48. https://doi.org/10.14341/probl11628
34. Doue, T., Ohtsuki, K., Ogawa, K., Ueda, M., Azuma, A., Saji, H., Strauss, H.W., and Matsubara, H., *J. Nucl. Med.*, 2008, vol. 49, pp. 1694–1700. https://doi.org/10.2967/jnumed.107.050260
35. Reischl, G., Dorow, D.S., Cullinane, C., Katsifis, A., Roselt, P., Binns, D., and Hicks, R.J., *J. Nuclear Med.*, 2007, vol. 43, pp. 365.
36. Rajendran, J.G., Wilson, D.C., Conrad, E.U., Peterson, L.M., Bruckner, J.D., Rasey, J.S., Chin, L.K., Hofstrand, P.D., Grierson, J.R., Eary, J.F., and Krohn, K.A., *Eur. J. Nuclear Med. Mol. Imaging*, 2003, vol. 30, pp. 695–704. https://doi.org/10.1007/s00259-002-1096-7
37. Bombardieri, E., Ambrosini, V., Aktolun, C., Baum, R.P., Bishof-Delaloye, A., Del Vecchio, S., Maffioli, L., Mortelmans, L., Oyen, W., Giovanna Pepe, G., and Chiti, A., *Eur. J. Nuclear Med. Mol. Imaging*, 2010, vol. 37, pp. 1441–1448. https://doi.org/10.1007/s00259-010-1473-6
38. Glaudemans, A.W.J.M., Enting, R.H., Heesters, M.A.A.M, Dierckx, R.A.J.O, van Rheenen, R.W.J., Walenkamp, A.M.E., and Slart, R.H.J.A., *Eur. J. Nucl. Med. Mol. Imaging*, 2013, vol. 40, pp. 615–635. https://doi.org/10.1007/s00259-012-2295-5

39. Lapa, C., Kircher, M., Da Via, M., Schreder, M., Rasche, L., Kortüm, K.M., Einsele, H., Buck, A.K., Hänscheid, H., and Samnick, S., *Clin. Nucl. Med.*, 2019, vol. 44, pp. 620–624. https://doi.org/10.1097/rlu.0000000000002638
40. Krause, B.J., Souvatzoglou, M., Tuncel, M., Herrmann, K., Buck, A.K., Praus, C., Schuster, T., Geinitz, H., Treiber, U., and Schwaiger, M., *Eur. J. Nucl. Med. Mol. Imaging*, 2008, vol. 35, pp. 18–23. https://doi.org/10.1007/s00259-007-0581-4
41. van de Wiele, C., Lahorte, C., Vermeersch, H., Loose, D., Mervillie, K., Steinmetz, N.D., Vanderheyden, J.L., Cuvelier, C.A., Slegers, G., and Dierck, R.A., *J. Clin. Oncol.*, 2003, vol. 21, pp. 3483–3487. https://doi.org/10.1200/jco.2003.12.096
42. Narula, J., Acio, E.R., Narula, N., Samuels, L.E., Fyfe, B., Wood, D., Fitzpatrick, J.M., Raghunath, P.N., Tomaszewski, J.E., Kelly, C., Steinmetz, N., Green, A., and Tait, J.F., *Nature Med.*, 2001, vol. 7, pp. 1347–1352. https://doi.org/10.1038/nm1201-1347
43. Hirata, K., Terasaka, S., Shiga, T., Hattori, N., Magota, K., Kobayashi, H., Yamaguchi, S., Houkin, K., Tanaka, S., Kuge, Y., and Tamaki, N., *Eur. J. Nucl. Med. Mol. Imaging*, 2012, vol. 39, pp. 760–770. https://doi.org/10.1007/s00259-011-2037-0
44. Shi, W., Wang, H.S., Pan, Z., Wymore, R.S., Cohen, I.S, McKinnon, D., and Dixon, J.E., *J. Physiol.*, 1998, vol. 511, pp. 675–682. https://doi.org/10.1111/j.1469-7793.1998.675bg.x